Low Temperature Physics/Fizika Nizkikh Temperatur, 2015, v. 41, No. 6, pp. 571–575

Poisson's ratio in cryocrystals under pressure

Yu.A. Freiman, Alexei Grechnev, and S.M. Tretyak

B. Verkin Institute for Low Temperature Physics and Engineering of the National Academy of Sciences of Ukraine
47 Lenin Ave., Kharkov 61103, Ukraine
E-mail: freiman@ilt.kharkov.ua

Alexander F. Goncharov

Geophysical Laboratory, Carnegie Institution of Washington, 5251 Broad Branch Road NW, Washington DC 20015, USA

Center for Energy Matter in Extreme Environments and Key Laboratory of Materials Physics, Institute of Solid State Physics, Chinese Academy of Sciences, 350 Shushanghu Road, Hefei, Anhui 230031, China

Eugene Gregoryanz

School of Physics and Centre for Science at Extreme Conditions, University of Edinburgh, Edinburgh EH9 3JZ, UK

Received February 18, 2015, published online April 23, 2015

We present results of lattice dynamics calculations of Poisson's ratio (PR) for solid hydrogen and rare gas solids (He, Ne, Ar, Kr and Xe) under pressure. Using two complementary approaches — the semi-empirical many-body calculations and the first-principle density-functional theory calculations we found three different types of pressure dependencies of PR. While for solid helium PR monotonically decreases with rising pressure, for Ar, Kr, and Xe it monotonically increases with pressure. For solid hydrogen and Ne the pressure dependencies of PR are nonmonotonic displaying rather deep minimums. The role of the intermolecular potentials in this diversity of patterns is discussed.

PACS: 67.80.F– Solids of hydrogen and isotopes;
67.80.B– Solid ^{4}He;
62.20.dj Poisson's ratio.

Keywords: Poisson's ratio, rare gas solids, solid hydrogen, intermolecular potential.

At low temperatures and pressures solid helium is an ultimate quantum solid displaying such phenomena as zero-temperature quantum melting and quantum diffusion. As atomic masses and interatomic forces increase in the sequence Ne, Ar, Kr, and Xe quantum effects in their properties become progressively less pronounced. Solid hydrogen is the only molecular quantum crystal where both translational and rotational motions of the molecules are quantum. Translational quantum effects decrease with increasing pressure.

Quantum and classical solids respond to the applied pressure differently. When pressure is applied to a classical solid the atoms are "pushed into" the hard cores of the potential; as a result of this core, the compressibility is usually quite small. Typically, the pressure of 1 GPa results in a few percent change in molar volume. At the same time, quantum solids hydrogen and helium are highly compressible. For hydrogen the pressure of 1 GPa results in a 100% change in volume. The physical reason for this is that the lattice is highly blown up due to the zero-point kinetic energy. The initial compression works against the weaker "kinetic pressure" rather than the harder "core pressure".

One of fundamental thermodynamic characteristics describing behavior of a material under mechanical load is Poisson's ratio [1,2]. For isotropic elastic materials the Poisson's ratio is uniquely determined by the ratio of the bulk modulus B to the shear modulus G, which relate to the change in size and shape respectively [3]:

$$\sigma = \frac{1}{2}\,\frac{3B/G - 2}{3B/G + 1}. \qquad (1)$$

As can be seen from this equation, PR can take values between –1 $(B/G \to 0)$ and 1/2 $(B/G \to \infty)$. The lower limit corresponds to the case where the material does not change

its shape and upper limit corresponds to the case when the volume remains unchanged. Materials with small PR (small B/G), such as cork, are more easily compressed than sheared, whereas those with PR approaching 1/2 (large B/G) are rubber-like: they strongly resist compression in favor of shear.

For most isotropic materials PR lies in the range $0.2 \le \sigma < 0.5$ [4]. Materials with $0 < \sigma < 0.2$ are rare — beryllium ($\sigma = 0.03$), diamond ($\sigma = 0.1$) — and are very hard [1]. Typically, PR increases with pressure near linearly with the rate $\partial\sigma/\partial P \sim 10^{-3}\,(\text{GPa})^{-1}$ indicating a continuous loss of shear strength [5–7].

An unusual pressure dependence of PR decreasing with rising pressure in solid hydrogen in the pressure range up to 24 GPa [8] and solid helium up to 32 GPa [9] was found by Zha *et al.* With the aim to investigate the distinctions in the response of quantum and classical solids to the applied pressure we calculated pressure dependencies of PR in the quantum (He, H_2, Ne) and classical (Ar, Kr, Xe) cryocrystals under pressure. The calculations were performed using complementary semi-empirical (SE) and density functional theory (DFT) with generalized gradient approximation (GGA) approaches. The DFT calculations were performed using the FP–LMTO code RSPt, while the SE calculations were done using our own code. The calculation details have been published previously [10]. It is important to notice that the two approaches treat solid hydrogen in fundamentally different ways. SE approach deals with interaction between H_2 molecules, which are treated as nearly spherically symmetrical quantum rotators, while the DFT can only treat fully oriented (classical) H_2 molecules, ignoring the zero-point rotations. The $Pca2_1$ oriented structure has been used for our calculations.

One of the signatures of a quantum crystal is that it melts at temperature T_m much lower the Debye temperature [11]:

$$\Theta_D/T_m >> 1. \qquad (2)$$

Figure 1 shows pressure dependencies of Θ_D and T_m for solid hydrogen, helium, neon, and argon. At zero pressure and temperature the ratio Θ_D/T_m is infinitely large for helium and 8.5 for parahydrogen. The ratio rather slowly decreases with rising pressure. For example, at 1 GPa it is still as high as 3.75 for helium and 3.0 for parahydrogen. For solid Ne at zero pressure Θ_D/T_m = 2.7 thus making solid Ne a candidate for the manifestation of quantum effects. Other RGS, with Θ_D/T_m = 1, 0.55, and 0.35 for Ar, Kr and Xe respectively, can be regarded as essentially classical solids.

Rewriting Eq. (1) in terms of the ratio of the bulk (hydrodynamic) v_B to the transverse (shear) sound velocity v_S we have [2]:

$$\sigma = \frac{1}{2}\frac{(v_B/v_S)^2 - 2}{(v_B/v_S)^2 - 1}. \qquad (3)$$

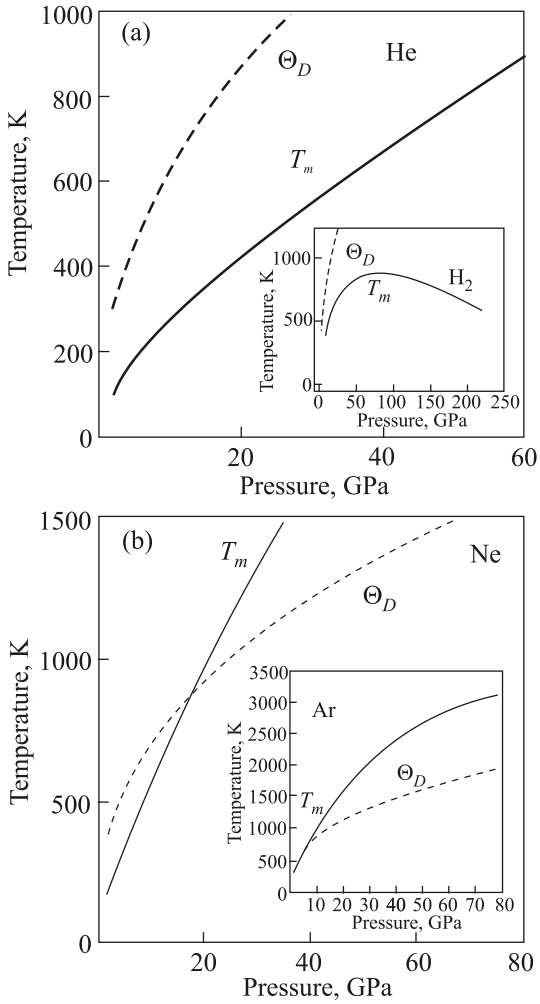

Fig. 1. Debye temperature and melting temperature vs pressure. He and H_2 (insert) (a); Ne and Ar (insert) (b). Experimental melting curves: He and Ne [12], Ar [13]. H_2 melting curve corresponds to Kechin Eq. [14]. Debye temperatures were calculated using the many-body potentials: for He and H_2 [10,15], for Ne and Ar [16].

The hydrodynamic or bulk sound velocity v_B can be found from Equation of State:

$$v_B = [\partial P/\partial \rho]^{1/2} = \left[-\frac{V^2}{\mu}\frac{\partial P}{\partial V}\right]^{1/2}, \qquad (4)$$

where P is pressure, μ is molar mass, and V is molar volume. In the calculations of v_B for H_2 we used our SE and DFT–GGA EOS from Ref. 17, for He, Ar and Xe from Refs. 16, 18, and for Kr from Ref. 19. We have also included zero-point vibrations in the Debye approximation in our calculations of $P(V)$ and $v_B(V)$ [10].

Generally, to find sound velocities v_P and v_S one has to find a complete set of elastic moduli C_{ij}. In the case of hcp lattice there is a simplified scheme based on lattice dynamics [20,21], which makes it possible to circumvent the problem of calculations of elastic moduli. In particular, in this approach it is possible to relate frequency ν of the

Raman-active E_{2g} phonon mode of hcp lattice and the shear elastic constant C_{44}:

$$C_{44} = \frac{1}{4\sqrt{3}} \frac{c}{a} \frac{m}{a} \nu^2(E_{2g}), \quad (5)$$

where a, c are the lattice parameters and m is the molecular mass. The pressure dependencies of $\nu(E_{2g})$ and C_{44} were found for H_2 [17] and hcp RGS (hcp He, Ar, Kr, and Xe) [18,22] using both *ab initio* DFT and SE lattice dynamics approaches. The shear velocity v_S was obtained using the relation

$$v_S = \sqrt{C_{44}/\rho}, \quad (6)$$

where ρ is the density, disregarding the elastic anisotropy of the crystal. A special case is solid Ne which preserves the fcc structure up to at least 208 GPa [23] which makes the outlined procedure impossible. For this reason for solid Ne we used results of lattice dynamics calculations by Gupta and Goyal [19].

The sound velocities for H_2 and He are given in Ref. 15; the data for Ne by Gupta and Goyal were published in Ref. 19; the data for Ar, Kr, and Xe will be published elsewhere. Pressure dependencies of Poisson's ratios for helium, hydrogen, neon, argon, krypton, and xenon calculated from sound velocities using Eq. (3) are shown in Figs. 2–5.

Figure 2 shows the pressure dependence of Poisson's ratio in solid He obtained in the framework of SE and DFT–GGA approaches in comparison with experimental results from Refs. 9, 24. Results which account for zero-point vibrations (ZPV) and those obtained disregarding ZPV are presented. Both SE and DFT–GGA calculations agree with the somewhat surprising experimental result of Poisson's ratio decreasing with pressure. There is a reasonable fair agreement between the SE theoretical curve (comprising ZPV) and experimental data. Usually SE results are preferable at smaller pressures while at higher pressures

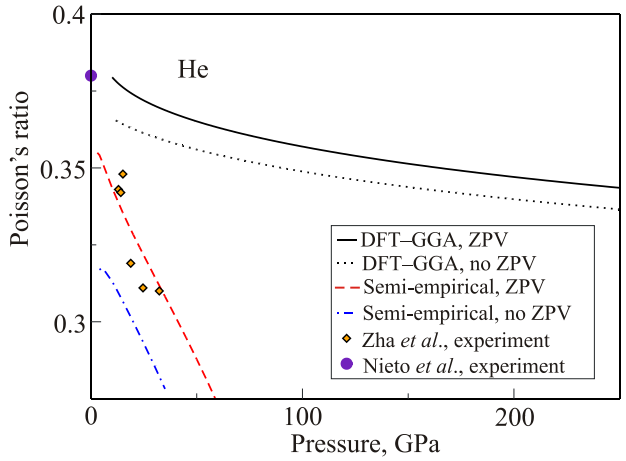

Fig. 2. (Color online). Poisson's ratio of solid He as a function of pressure. Theory: this work. Experiment: Zha *et al.* [9]; Nieto *et al.* [24].

the DFT approach works better. Comparing the SE and DFT theoretical curves it is hard to say in which way the low-pressure SE results could continuously go over to the high-pressure DFT ones. It should be noted that the experimental points may show that around 30 GPa there is a minimum point at the pressure dependence of PR.

As was said above, typically [5–7] Poisson's ratio increases with pressure and tends to 1/2 (the limit of zero compressibility) when pressure goes to infinity. It would appear reasonable to consider anomalous behavior of PR in such quantum solids as He and H_2 as a manifestation of quantum effects. Reasons for such understanding is the following. It is known that the He and H_2 lattices are swelled due to large zero-point vibrations (ZPV). If ZPV were not present, "classical" solid He and H_2 would have much smaller zero molar volumes ($V_0^{cl}(\mathrm{He}) \approx 11.2$ cm^3/mol; $V_0^{cl}(\mathrm{H_2}) \approx 7.4$ cm^3/mol), i.e., the swelling effect is huge [18]. Until the volume reaches about V_0^{cl}, the main effect of the external pressure is the suppression of the zero-point vibrations and not the compression of the electron shells.

To check whether this explanation is correct we calculated PR of He disregarding ZPV, that is, for "classical" He both in the SE and DFT approaches (dot-dash and dotted curves, respectively, Fig. 2). As can be seen, the pressure dependence of PR with and without ZPV is qualitatively the same. Thus, the anomalous (descending with rising pressure) behavior of PR is not a quantum effect. As can be seen from Fig. 2, the contribution of ZPV into PR is positive. This fact is easily understood if we take into account that the introduction of ZPV is a step to liquation but PR of liquid is an upper bound for PR of any substance. Naturally, the relative value of this contribution increases with decreasing pressure and as pressure goes to zero it increases up to 15%. The effect of ZPV is much higher in the case of ^{3}He. Nieto *et al.* [24] showed that the mixture ^{3}He–^{4}He has higher PR than pure ^{4}He. For pure ^{3}He they gave value of PR 0.473 rather close to the liquid limit.

The theoretical and experimental pressure dependencies of PR for solid H_2 are shown in Fig. 3. As can be seen, the SE and DFT–GGA approaches give the opposite signs of the pressure effect on PR: PR decreases with rising pressure for SE and increases for DFT–GGA. Since in the experimentally studied pressure range (up to 24 GPa) the SE result agrees qualitatively with experiment [8], we conclude that at low pressures PR decreases with rising pressure for solid H_2. It is known that while the SE approach works well for molecular solids at low pressures, for higher pressures the DFT–GGA approach is preferable. Thus the PR(P) curve can be subdivided into three regions: At the low-pressure region SE is expected to work well, while at high pressures we can use the DFT–GGA approach. In the intermediate pressure range both approaches fail. The dot-dot dash curve shows schematically a possible continuous transition from the low-pressure asymptote to high-pressure one. Resulting pressure dependence of PR for H_2 is nonmonotonic dis-

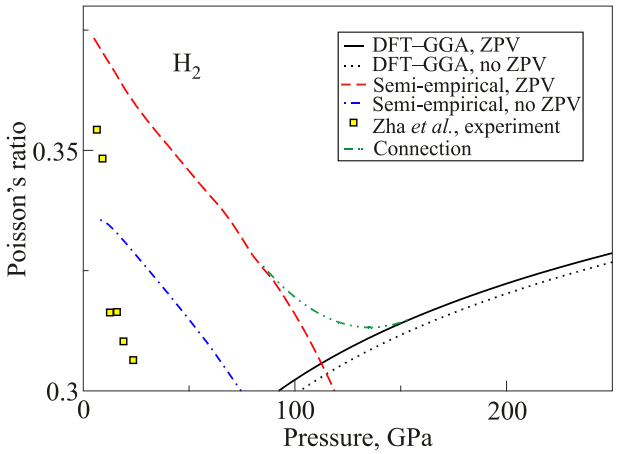

Fig. 3. (Color online). Poisson's ratio of solid H_2 as a function of pressure. Theory: this work. Experiment: Zha *et al.* [8]

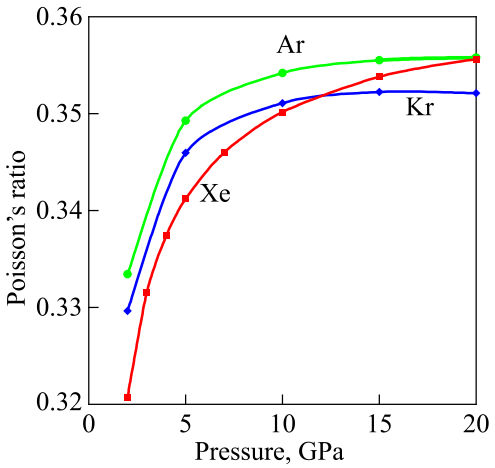

Fig. 5. (Color online) Poisson's ratio of solid Ar, Kr, Xe as a function of pressure. Calculated using SE data on sound velocities (unpublished).

playing rather deep minimum. It should be noted that the transient region from the descending to the ascending curves falls on phase II of the hydrogen phase diagram. As mentioned above, the SE and DFT approaches treat the orientational degrees of freedom in H_2 in completely different ways: the former regards H_2 molecules as nearly spherically symmetric quantum rotators (as in phase I), while the latter considers classically oriented H_2 molecules (as in phase III), completely ignoring any quantum rotations or librations. It seems likely that this is the reason why SE and DFT give such drastically different PR(P) curves for H_2, while results for helium are qualitatively similar. It would mean that the PR minimum in hydrogen is related to the orientational transition at around 110 GPa, however more detailed study of this question is beyond the scope of the present work.

A similar curve with a deep minimum was obtained for PR in solid neon (Fig. 4). The pressure dependence of PR was obtained from the SE theoretical results on sound velocities obtained by Gupta and Goyal [19]. Unfortunately, experimental data on sound velocities in solid Ne exist for very narrow pressure range 5–7 GPa [25]. In this region PR ≈ 0.37.

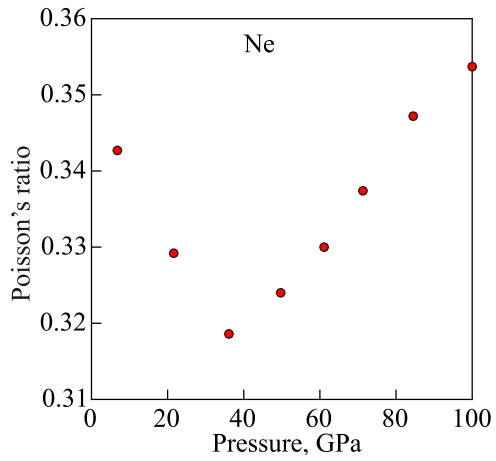

Fig. 4. (Color online) Poisson's ratio of solid Ne as a function of pressure. Calculated using data on sound velocities by Gupta and Goyal [19].

Figure 5 shows the pressure dependencies of PR obtained in the SE approach for Ar, Kr, and Xe. In contrast with He, H_2, and Ne, we obtained that PR for the heavy RGS increases with rising pressure.

In conclusion, we present results of lattice dynamics calculations of Poisson's ratio for solid hydrogen and rare gas solids (He, Ne, Ar, Kr and Xe) under pressure. Using two complementary approaches: lattice dynamics based on the semi-empirical many-body potentials and *ab initio* DFT–GGA we found three different types of the behavior of PR with pressure. While for solid He PR monotonically decreases with rising pressure, for Ar, Kr, and Xe it monotonically increases with pressure. For solid H_2 and Ne PR are nonmonotonic with pressure displaying rather deep minimums. To investigate the role of quantum effects we performed the calculations of PR disregarding zero-point vibrations and found qualitatively similar results, that is, we proved that the effects have a nonquantum origin. We may rather say that the anomalies, discovered for H_2, He and Ne, and quantum effects in these cryocrystals have common origins: weak intermolecular interactions and small masses of constituent atoms and molecules.

We thank J. Peter Toennies for valuable discussions.

1. G.N. Greaves, A.L. Greer, R.L Lakes, and T. Rouxel, *Nature Mater*. **10**, 823 (2011).
2. *Physics of Cryocrystals*, V.G. Manzhelii and Yu.A. Freiman (eds.), AIP Press, New York (1997).
3. J-P. Poirier, *Introduction to the Physics of the Earth's Interior*, Cambridge Univ. Press (2000).
4. P.H. Mott and C.M. Roland, *Phys. Rev. B* **80**, 132104 (2009).

5. G. Steinle-Neumann, L. Stixrude, and R.E.Cohen, *Phys. Rev. B* **60**, 791 (1999).
6. C.-S. Zha, H.-k. Mao, R.J. Hemley, and Y. Wu, *PNAS* **97**, 13494 (2000).
7. D. Antonangeli, M. Krisch, G. Fiquet, J. Badro, D. L. Farber, A. Bossak, and S. Merkel, *Phys. Rev. B* **72**, 134303 (2005).
8. C.S. Zha, T.S. Duffy, H.-k. Mao, and R.J. Hemley, *Phys. Rev. B* **48**, 9246 (1993).
9. C.S. Zha, H.-k. Mao, and R.J. Hemley, *Phys. Rev. B* **70**, 174107 (2004).
10. Yu.A. Freiman, Alexei Grechnev, S.M. Tretyak, Alexander F. Goncharov, C.-S. Zha, and R.J. Hemley, *Phys. Rev. B* **88**, 214501 (2013).
11. William B. Daniels, in: *Simple Molecular Systems at Very High Density*, A. Polian, P. Loubeyre, and N. Boccara (eds.), Plenum Pres, New York and London, (1989), pp. 13–31. W.B. Daniels, Helium phase diagram
12. David Santamaria-Pérez, Goutam Dev Mukherjee, Beate Schvager, and Reinhard Boehler, *Phys. Rev. B* **81**, 214101 (2010).
13. R. Boehler, M. Ross, Per Söderlind, and David B. Boercker, *Phys. Rev. Lett*. **86**, 5731 (2001).
14. V.V. Kechin, *J. Phys.: Condens. Matter* **7**, 531 (1995).
15. Yu.A. Freiman, Alexei Grechnev, S.M. Tretyak, Alexander F. Goncharov, and Russell J. Hemley, *Fiz. Nizk. Temp*. **39**, 548 (2013) [*Low Temp. Phys*. **39**, 423 (2013)].
16. Yu.A. Freiman and S.M. Tretyak, *Fiz. Nizk. Temp*. **33**, 719 (2007) [*Low Temp. Phys*. **33**, 545 (2007)].
17. Yu.A. Freiman, A. Grechnev, S.M. Tretyak, Alexander F. Goncharov, and R.J. Hemley, *Phys. Rev. B* **86**, 014111 (2012).
18. Yu.A. Freiman, A.F. Goncharov, S.M. Tretyak, A. Grechnev, J.S. Tse, D. Errandonea, H.-k. Mao, and R.J. Hemley, *Phys. Rev. B* **78**, 014301 (2008).
19. S. Gupta and S.C. Goyal, *Sci. China, Ser. D-Earth Sci*. **52**, 1599 (2009).
20. E.A. Metzbower, *Phys. Status Solidi* **25**, 403 (1968).
21. H. Olijnyk and A.P. Jephcoat, *J. Phys.: Condens. Matter* **12**, 10423 (2000).
22. H. Shimizu, M. Kawajiri, T. Kume, S. Sasaki, Yu.A. Freiman, and S.M. Tretyak, *Phys. Rev. B* **79**, 132101 (2009).
23. A. Dewaele, F. Datchi, P. Loubeyre, and M. Mezouar, *Phys. Rev. B* **77**, 094106 (2008).
24. P. Nieto, G. Benedek, and J. Peter Toennies, *New J. Phys*. **14** 013007 (2012).
25. H. Shimizu, H. Imaeda, T. Kumew, and S. Sasaki, *Phys. Rev. B* **71**, 014108 (2005).